The Journal of Neuroscience, August 1, 1998, *18*(15):5859–5868

# The Effect of the Mouse Mutation *Claw Paw* on Myelination and Nodal Frequency in Sciatic Nerves

**Adam G. Koszowski,[1] Geoffrey C. Owens,[2,3] and S. Rock Levinson[1,3]**

*Departments of [1]Physiology and Biophysics and [2]Biochemistry and Molecular Genetics and [3]Program in Neuroscience, University of Colorado Health Sciences Center, Denver, Colorado 80262*

Despite the biophysical and clinical importance of differentiating nodal and internodal axolemma, very little is known about the process. We chose to study myelination and node of Ranvier formation in the hypomyelinating mouse mutant *claw paw* (*clp*). The phenotype of *clp* is delayed myelination in the peripheral nervous system. The specific defect is unknown but is thought to arise from a breakdown in the complex signaling mechanism between axon and Schwann cell. Myelination was assessed in sciatic nerve cross sections from adult and postnatal day 14 (P14) heterozygous and homozygous *clp* mice. Antibodies to P0, myelin-associated glycoprotein (MAG), and neural cell adhesion molecule were used to assess the stage of myelination. P14 homozygous *clp* mice showed an atypical staining pattern of immature myelin, which resolved into a relatively normal pattern by adulthood. Sodium channel clustering and node of Ranvier frequency were studied in whole-mount sciatic nerves with sodium channel and MAG antibodies. P14 homozygous *clp* nerves again showed an atypical, immature pattern with diffuse sodium channel clusters suggesting nodal formation was delayed. In the adult, homozygous *clp* sciatic nerves displayed dramatically shortened internodal distances. The data from this study support the hypotheses that node of Ranvier formation begins with the onset of myelination and that the number and location of nodes of Ranvier in the sciatic nerve are determined by myelinating Schwann cells.

*Key words: internodal length;* claw paw*; sciatic nerve; node of Ranvier; sodium channel; immunocytochemistry; MAG; NCAM; P0*

An alternating pattern of myelinating glia and nodal architecture is required for saltatory conduction in myelinated nerves. The key functional elements in this nodal architecture are voltage-gated sodium channels, which are highly concentrated at nodes of Ranvier but are diffuse along internodal axolemma. The means by which nodal and internodal axolemma are differentiated, however, remains to be discerned. It is generally agreed that a molecular dialogue must take place between the neuron and glia for normal nodal development, and there has been a lot of interest in the details of this axon–glia interaction (for review, see Salzer, 1997). An important question about this interaction concerns whether the location of nodes is determined by neurons or myelinating glia.

Several investigators have examined this question with conflicting results. Sodium channel distribution was examined immunocytochemically in normal rat sciatic nerves during development (Vabnick et al., 1996) and during remyelination (Dugandzija-Novakovic et al., 1995). In both cases, axonal sodium channel clusters were found at the ends of Schwann cells that had just started myelinating, and the clusters seemed to get "pushed" by these elongating Schwann cells until stable nodal gaps were formed by adjacent Schwann cells. These observations are strong evidence that myelinating Schwann cells determine the location of nodes of Ranvier in the peripheral nervous system (PNS).

The alternate hypothesis that axons predetermine nodal sites has support in a study of sodium channel distribution in cultured retinal ganglion cells (Kaplan et al., 1997). This study showed that sodium channels could be organized along neuronal processes into node-like clusters at the expected spatial frequency with only cell-free, oligodendrocyte-conditioned media. This observation suggests that neurons determine the location of nodes on CNS axons. Support for this hypothesis in the PNS has come from two studies. Deerinck et al. (1997) studied sodium channel distribution in spinal roots of dystrophic mice. These roots have fiber bundles that are devoid of Schwann cells, yet irregularly spaced sodium channel clusters were found on bare axolemma. Furthermore, Lambert et al. (1997) found that in developing rodent sciatic nerves, ankyrin-binding proteins were clustered at sites independent of myelinating Schwann cells.

In a further attempt to shed some light on the question of which cell type determines the location of nodes of Ranvier in PNS neurons, we chose to study the hypomyelinating mouse mutant *claw paw* (*clp*). *clp* is an autosomal recessive mutation of an unknown gene resulting in a delay in the onset of myelination in the PNS with no obvious ultrastructural axonal abnormalities or evidence of ongoing demyelination and remyelination (Henry et al., 1991). It is hypothesized that this delay is attributed to a breakdown in the complex signaling mechanism between axon and Schwann cell. If this interaction were required for the specification of nodal sites, then one would expect nodal location to be altered temporally and spatially in *clp* nerves. Thus, we examined the frequency of nodes and the expression of myelin markers in sciatic nerves from *clp* mice.

## MATERIALS AND METHODS

### *Mouse breeding*

Six heterozygote *clp*/C57BL mice, obtained from The Jackson Laboratory (Bar Harbor, ME), were bred, and the progeny were screened for homozygotes. *clp* homozygotes were identified within 2 d of birth by the

Received Feb. 17, 1998; revised May 5, 1998; accepted May 12, 1998.

This work was supported by National Institutes of Health Grant NS34375. We thank Dr. Robin Michaels for assistance with cryostat sectioning, Dawn Hilton for care of the mice, and Dr. Margaret Neville for assistance with this manuscript.

Correspondence should be addressed to Adam Koszowski, 4200 East Ninth Avenue, Box C240, Denver, CO 80262.

 0270-6474/98/185859-10$05.00/0

characteristic retracted forelimbs (Henry et al., 1991). Heterozygotes were generated by breeding homozygous *clp* females with wild-type C57BL/6 males.

### *Sciatic nerve immunocytochemistry*

*Antibody and general immunocytochemistry.* The following primary antibodies were used in this study: anti-myelin associated glycoprotein (MAG), monoclonal cell line 513 from mouse (Boehringer Mannheim, Indianapolis, IN), anti-neural cell adhesion molecule (NCAM), monoclonal cell line H28 from rat (Boehringer Mannheim), anti-P0, polyclonal from rabbit (from Jeremy Brockes, Ludwig Institute for Cancer Research), anti-sodium channel, and AP-1380-3.1 polyclonal from rabbit (peptide antigen, TEEQKKYYNAMKKLGSKK; Dugandzija-Novakovic et al., 1995). Secondary antibodies used in this study were donkey anti-rabbit lissamine–rhodamine (Jackson ImmunoResearch, West Grove, PA), goat anti-rat FITC (Jackson ImmunoResearch), and donkey anti-mouse FITC (Jackson ImmunoResearch). All washes were performed in PBS, and incubations were done at room temperature unless otherwise noted. Slides were mounted with Vectastain photoprotecting media (Vector Laboratories, Burlingame, CA), and all data collection was performed on a Bio-Rad (Hercules, CA) laser scanning confocal microscope (MRC-600). Digital images were reproduced on an Eastman Kodak (Rochester, NY) 8650 dye sublimation printer.

*Cross-sections.* Mice were anesthetized with halothane and decapitated. Both sciatic nerves were removed at the level of the femur and flash frozen in OCT. Ten-micrometer serial cryostat sections were collected onto Superfrost Plus glass slides (Fisher Scientific, Pittsburgh, PA) and allowed to dry. Slides were stored at −20°C until they were processed for immunocytochemistry. The slides were thawed, and then one of two different immunostaining protocols was used depending on the primary antibody. Sections to be stained with the anti-NCAM monoclonal antibody were thawed and fixed with 3.7% formaldehyde in 0.12 M sucrose in PBS. The slides were then washed and placed in a humidified incubation chamber. Nonspecific protein binding sites were blocked, and the tissue was permeabilized with a blocking solution consisting of 4% normal donkey serum, 2% bovine γ-globulin, and 0.4% Triton X-100 in PBS (BS+T). Primary antibodies (anti-NCAM at 1:100 and anti-P0 at 1:200) were diluted in BS+T and allowed to react overnight. Slides were washed again, and secondary antibodies were diluted in BS+T, filtered, and applied. After washing, slides were rinsed in distilled water and mounted. Sections to be stained with the anti-MAG monoclonal antibody were thawed and fixed with 3.7% formaldehyde in 0.12 M sucrose in PBS. The slides were then washed, permeabilized with 100% methanol, washed again, and then placed in a humidified incubation chamber. Nonspecific protein binding sites were blocked with a blocking solution consisting of 12% normal donkey and goat serum in PBS (BS−T) for at least 1 hr. Primary antibodies (anti-MAG at 1:20 and anti-P0 at 1:200) were diluted in BS−T and allowed to react overnight. Slides were washed again, and secondary antibodies were diluted in BS−T, filtered, and applied to the slides. After washing in PBS, slides were rinsed in distilled water and mounted.

*Whole mounts.* Mice were anesthetized with halothane and decapitated. Both sciatic nerves were removed at the level of the femur and fixed for 30 min in 4% paraformaldehyde in PBS. After rinsing in 50% PBS, ~3 mm lengths of nerve were teased onto Fisher Superfrost Plus glass slides and allowed to dry. Slides were stored at −20°C until they were processed for immunocytochemistry. The slides were thawed, rinsed, and placed in a humidified incubation chamber. Nonspecific protein binding sites were blocked, and the tissue was permeabilized with BS+T for at least 1 hr. Primary antibodies were diluted in BS+T and allowed to react overnight. The sodium channel polyclonal antibody (AP-1380-3.1) and its blocked control were used at 1:100. Blocking of the sodium channel antibody was achieved by incubating 5 μl of undiluted antibody with 1 μl of its peptide antigen overnight at 4°C or for 4 hr at room temperature. The anti-MAG monoclonal antibody was used at 1:10. Slides were washed again, and secondary antibodies were diluted in BS+T, filtered, and applied. After washing in PBS, slides were rinsed in distilled water and mounted.

### *Internodal length measurement*

*Conventional.* After sodium channel immunocytochemistry on whole-mount sciatic nerves, as described above, the Bio-Rad confocal microscope program COMOS scale bar was used to measure node-to-node distances from a randomly selected pool of fibers in single images or montages.

*Statistical.* After double staining whole-mount sciatic nerves for sodium channels and MAG, as described above, positive MAG immunoreactivity was used to confirm that the fiber of interest was myelinated. Individual myelinated fibers that could be followed for >400 μm were measured. The number of nodes for that length was counted. Individual measurements were then summed, and dividing the number of nodes by total fiber length gave the nodal frequency, whose inverse is the mean internodal length. Fiber diameters were measured with the COMOS scale bar at a point just adjacent to the nodal swelling. Errors attributed to the stochastic nature of nodal occurrence were calculated using Poisson statistics in which the coefficient of variation was the inverse of the square root of the number of nodes counted. Errors attributed to length measurement were found to be relatively insignificant and have been ignored.

## RESULTS

### Myelin marker immunostaining of sciatic nerve cross-sections

#### *Adult heterozygotes*

Immunostaining for P0 in sciatic nerve cross-sections from adult heterozygous animals showed the expected ring-like pattern of bright-staining compact myelin around dark axoplasm (Fig. 1*A*) (Sternberger et al., 1979). Lawns of rings were interrupted by large areas with no P0-positive staining, presumably representing large bundles of unmyelinated fibers. These bundles stained with an antibody to NCAM, a marker present only on unmyelinated fibers (Martini and Schachner, 1986). A representative NCAM field is shown in Figure 1*E*, in which the irregular bright patches reflect bundles of unmyelinated nerve fibers. Adult heterozygote sciatic nerve cross-sections were also stained with a monoclonal antibody against MAG. MAG staining was localized to the periaxonal uncompacted myelin in myelinated fibers (Fig. 1*C*), as seen in the small rings distributed throughout the section. Double labeling with P0 and MAG confirmed that there was an outer P0-positive ring of compact myelin and an inner MAG-positive ring of uncompacted myelin (data not shown).

#### *Adult homozygotes*

Adult homozygous *clp* sciatic nerve cross-sections showed a staining pattern with both P0 and MAG that was very similar (except for the dark areas, see below) to that of nerve sections from heterozygotes (Fig. 1*B,D*). NCAM immunoreactivity, however, appeared different in the *clp* nerves (Fig. 1*F*). NCAM-positive staining was still present in unmyelinated fiber bundles but appeared to be associated with smaller bundles in the mutant compared with the heterozygote (Fig. 1, compare *F*, *E*). This observation was confirmed in the P0-stained sections by noting that the regions free of P0 were larger in the heterozygote than the homozygote (Fig. 1, compare *A*, *B*). Smaller NCAM bundles in the homozygote suggests that *clp* may have an altered time course of fiber sorting (i.e., fasciculation).

#### *P14 heterozygotes*

Nerves from P14 heterozygotes stained with P0 resembled their adult counterparts, showing relatively uniform staining of myelinated nerves as rings throughout the section (Fig. 2*A*). Likewise, the MAG staining (Fig. 2*C*) and NCAM staining (Fig. 2*E*) in the P14 heterozygote mirrored the staining pattern in the adult heterozygote. These observations suggest that in the heterozygote myelination is nearly complete by P14. The only difference observed between the P14 and adult heterozygote sections was one of size, because P14 sciatic nerves were smaller than adult sciatic nerves.

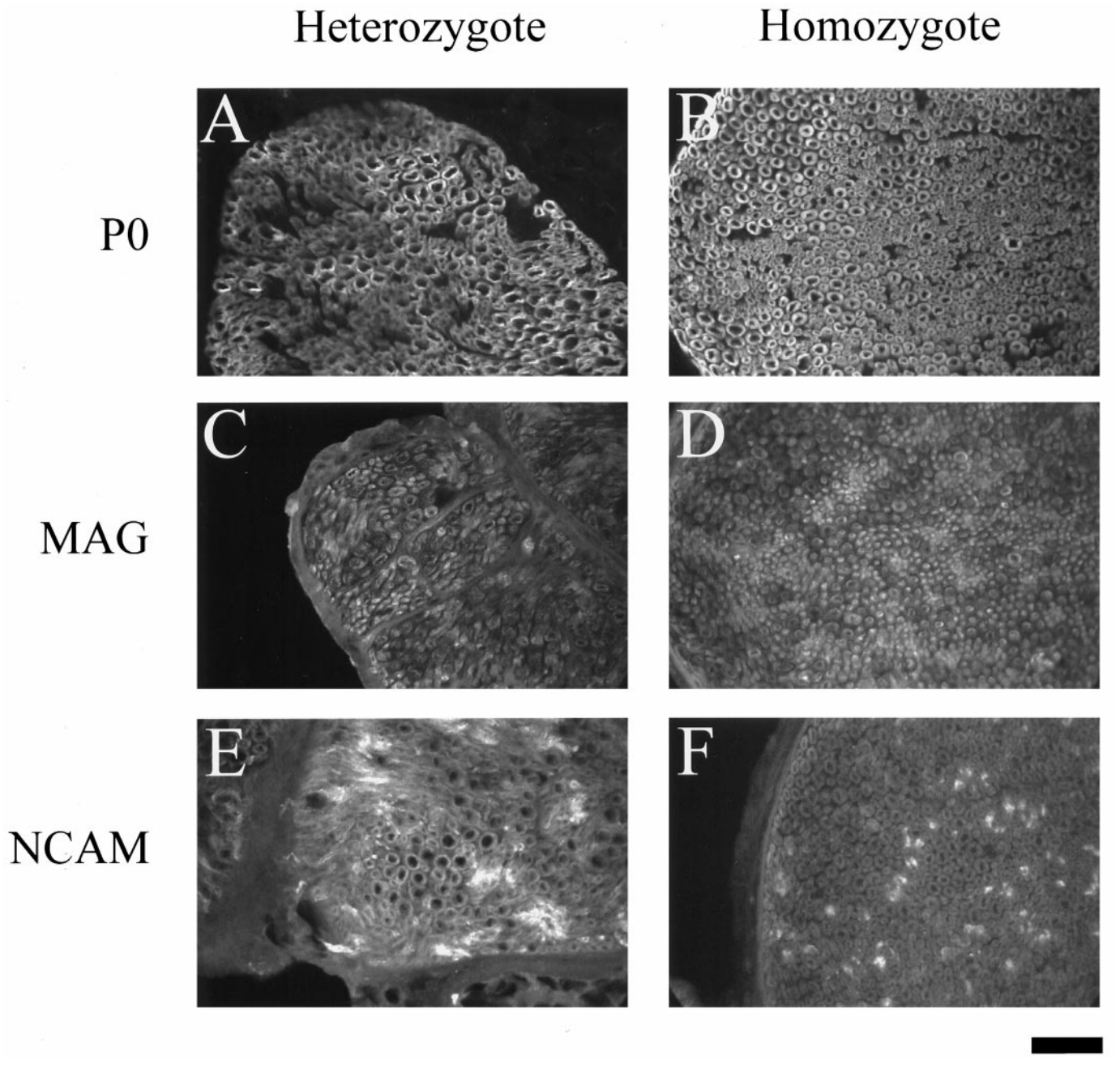


*Figure 1.* Adult sciatic nerve cross-sections. P0, MAG, and NCAM immunostaining of cross-sectioned sciatic nerves from heterozygous (*A, C, E*) and homozygous (*B, D, F*) adult mice is shown. Note a similar staining pattern is seen in heterozygote and homozygote with P0 (*A, B*) and MAG (*C, D*). NCAM gives a slightly different pattern in the homozygote (*F*) than in the heterozygote (*E*). Ten-micrometer cryostat sections; scale bar, 50 μm.

*P14 homozygotes*

In contrast to the heterozygote, the pattern of P0, MAG, and NCAM staining in the P14 homozygote suggested that myelination was still in the initial stages. P0 and MAG, for example, were present only in a small number of fibers (Fig. 2*B,D*). More specifically, MAG was present in the same P0-positive fibers and a few additional fibers, as seen when sections were costained for P0 and MAG. Thus, in Figure 2, *B* and *D* are the same section costained for P0 and MAG and visualized with different fluorophore-labeled secondary antibodies. Notice the central region of Figure 2*D* in which there are some MAG-positive fibers that are not P0-positive (*arrows*). This observation shows that MAG is expressed during the early stages of myelin wrapping before compaction in the *clp* homozygote. On the other hand, a higher level of NCAM immunoreactivity (Fig. 2*F*) was seen throughout the section compared with the heterozygote (Fig. 2*E*), suggesting that most of the nerve fibers in the P14 *clp* were still in a premyelinated state.

Overall, the above results strongly suggest that myelination is delayed in sciatic nerves from *clp* homozygotes. The next question was whether the myelination delay affected the relative location of nodes of Ranvier. Whole mounts of sciatic nerve were used rather than cross-sections so that nodes could be more easily observed and internodal lengths could be measured.

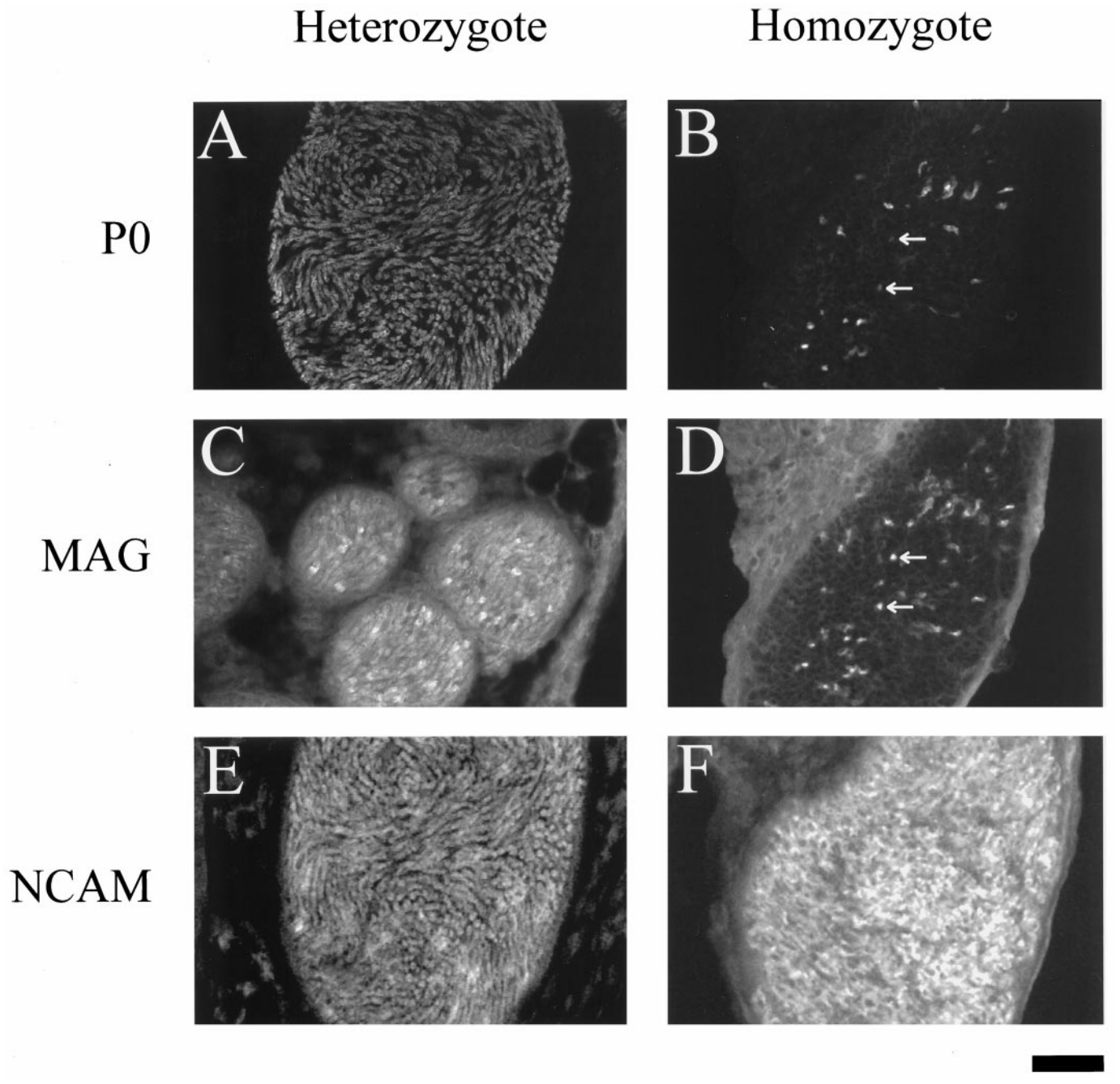


*Figure 2.* P14 sciatic nerve cross-sections. P0, MAG, and NCAM immunostaining of cross-sectioned sciatic nerves from heterozygous (*A, C, E*) and homozygous (*B, D, F*) 14-d-old mice is shown. Note that there are differences in each set of panels between the heterozygote and the homozygote. P14 homozygote has less P0 (*A* vs *B*) and less MAG (*C* vs *D*),but more NCAM (*E* vs *F*) than the P14 heterozygote. *Arrows* in *B* and *D* mark corresponding regions. Ten-micrometer cryostat sections; scale bar, 50 $\mu$m.

### Sodium channel immunostaining of sciatic nerve whole mounts

*P14 heterozygotes*

P14 sciatic nerve whole mounts were costained with our sodium channel polyclonal antibody and an anti-MAG monoclonal antibody (see Materials and Methods). The P14 heterozygote had the expected pattern for mature myelin. MAG was restricted to Schmidt–Lanterman incisures and paranodes (Fig. 3*C*). Sodium channels were found at nodes of Ranvier, identified by concentrated sodium channel staining (*arrows*) and MAG-positive paranodes. Sodium channels were also found diffusely distributed along unmyelinated fiber bundles (Fig. 3*A*, *open arrows*). These staining patterns support the data from cross-sections showing that myelination and node formation appear to be complete by P14 in the heterozygote.

*P14 homozygotes*

Figure 3*B* shows that there are sodium channel clusters (*arrows*); however, they are more diffuse than nodes in the heterozygote. By correlating with MAG staining (Fig. 3*D*), these sodium channel

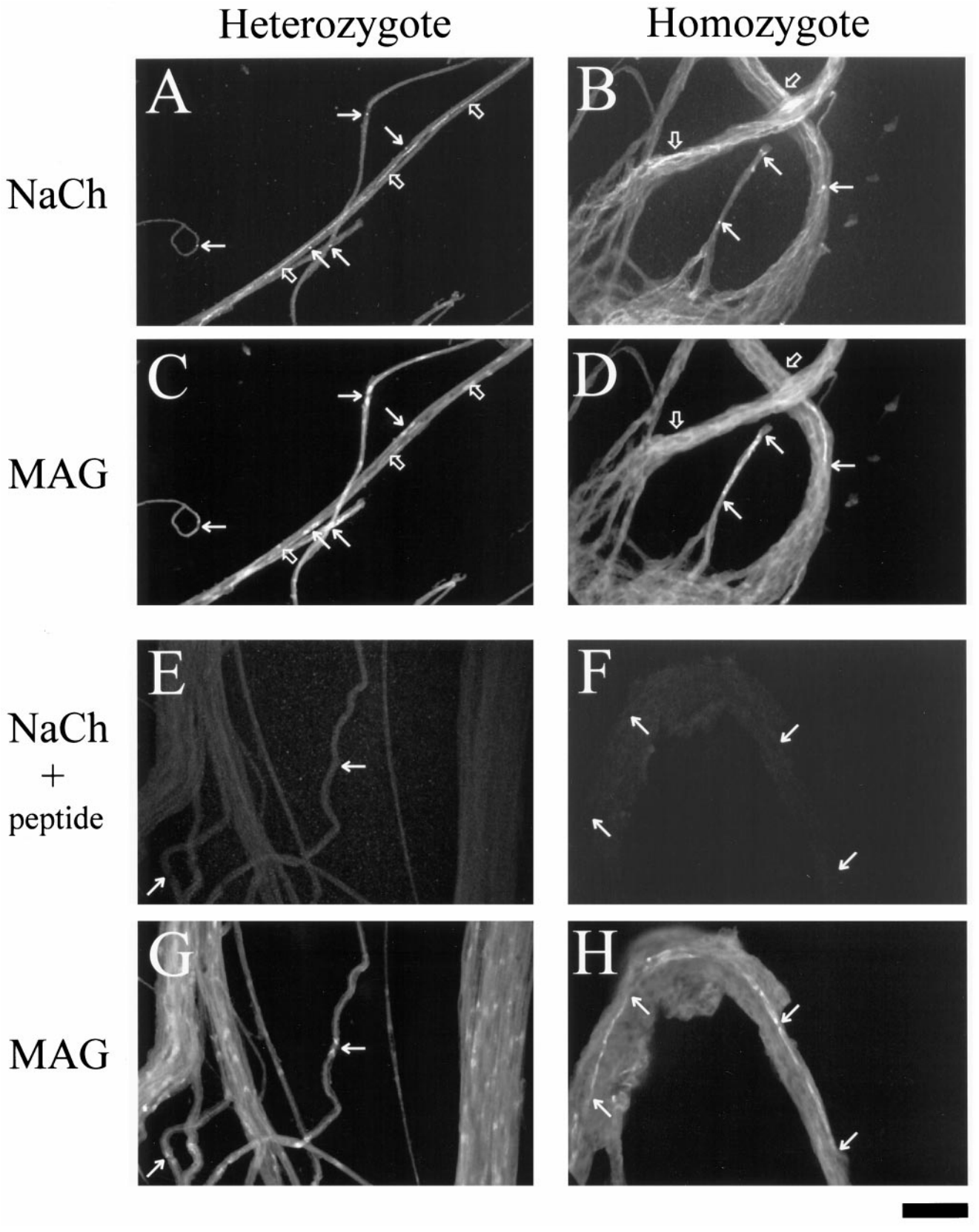


*Figure 3.* P14 sciatic nerve whole mounts. Sodium channel and MAG coimmunostaining of whole-mount sciatic nerves from heterozygous (*A*, *C*) and homozygous (*B*, *D*) P14 mice is shown. *Insets* are higher-magnification views of areas within the panels. *E* and *G* are heterozygote and *F* and *H* are homozygote sciatic nerves costained with MAG and the sodium channel antibody that had been preabsorbed with its peptide antigen. *Arrows* point to nodes of Ranvier and the corresponding locations in MAG-stained fields. *Open arrows* point to unmyelinated fibers and their corresponding locations in MAG stained fields. Scale bar, 50 $\mu$m.

aggregations appear to be localized to the ends of myelinating Schwann cells. In Figure 3, comparing *B* and *D* also shows that there were no sodium channel clusters other than those associated with MAG-positive Schwann cells, and low-level linear sodium channel staining occurred in some regions where there were no MAG-positive fibers (*open arrows*). Fibers that had no MAG staining were unmyelinated axons that may or may not become myelinated later. The stage of the myelin present in P14 homozygote fibers could be assessed by the pattern of MAG immunoreactivity. Figure 3, *D* and *H*, shows that MAG was expressed linearly along the Schwann cell length, which is a hallmark of precompacted early myelin (contrast the linear MAG staining pattern of the homozygote with the mature myelin pattern of MAG-positive paranodes and Schmidt–Lanterman incisures; Fig. 3*C*).

Figure 3, *E* and *F*, shows controls for the sodium channel antibody specificity. Figure 3*E* is a P14 heterozygote nerve costained just as in Figure 3*A*; however, the sodium channel antibody has been preincubated with its peptide antigen. Blocked and unblocked digital images (Fig. 3*A*,*E*) were treated identically. Figure 3*G* is the corresponding MAG-stained image showing several paranodal regions with no specific nodal sodium channel staining in Figure 3*E* above. Figure 3, *F* and *H*, shows a pair of blocked sodium channel and MAG antibody stainings of P14 homozygote nerves. Here, no sodium channel clusters are seen at the ends of MAG-positive Schwann cells, nor is there any linear sodium channel staining in regions without MAG.

*Adult heterozygotes*

These fibers were costained as before with sodium channel and MAG antibodies. Figure 4 shows four different fields of sodium channel immunocytochemistry of adult heterozygote sciatic nerves. *Arrows* denote nodes of Ranvier used to measure the internodal length. Figure 4*A–C* gives node-to-node measurements of internodal length. Figure 4*D* shows an example of a broken fiber, which presents a problem in the use of node-to-node measurements that is addressed below.

*Adult homozygotes*

Figure 5 has four different fields showing sodium channel immunocytochemistry in adult homozygote sciatic nerves. *Arrows* again denote nodes of Ranvier used to measure internodal length, with those distances given. Comparing Figures 4 and 5, one can see readily that the homozygote appears to have shorter internodes than the heterozygote in the examples given. In the next section, these and similar data are quantitated.

### Internodal distance estimates through measurement of nodal spatial frequency

Quantitation of the homozygote internodal distance using node-to-node measurements was straightforward, because complete internodes were present on most fibers imaged. The heterozygote proved to be more challenging because of the much longer internodal distances, which made following an intact fiber from one node to the next difficult. As shown in Figure 4*D* the nerve fibers often broke before a second node was seen, and broken fibers could not be included in the node-to-node measurement data shown in Table 1. Excluding these data biases the internodal measurements to the shorter, measurable internodes only. In an attempt to obtain a more accurate reflection of the true internodal lengths, a statistical technique was used. Individual myelinated fibers were followed as far as possible, and the total number of nodes was counted. MAG costaining was used to help identify nodes of Ranvier and myelinated fibers. Table 2 shows the measurements and calculated internodal lengths for adult heterozygote and homozygote nerves. Using nodal frequency to determine internodal length revealed a larger difference between heterozygote and homozygote internodes than node-to-node measurements, as expected from the bias effect discussed above (compare Tables 1, 2).

It was next considered whether this internodal length difference could be explained by changes in fiber diameter. Internodal length varies with fiber diameter and has been shown to be ~100 times total fiber thickness (Waxman, 1978). To determine whether abnormal *clp* homozygote internodal lengths were caused by an altered fiber diameter profile or nonrandom selection of nerve fibers, fiber diameter was measured along with nodal frequency. Wild-type nerves were also analyzed to ensure that possible semidominant expression of the *clp* mutation was not affecting the results (Henry et al., 1991).

Mean internodal length increased significantly with fiber diameter for the heterozygote and the wild type but not the homozygote (Fig. 6). Also analyzed were the number and percentage of fibers measured for each fiber diameter (Table 3). For example, four homozygote fibers were measured that had a diameter of 2 $\mu$m and a mean internodal length of 263 $\mu$m. These four 2 $\mu$m fibers represent 5% of the total fibers measured of all diameters in the homozygote. From the results obtained, it was concluded that all of the fiber diameters were represented in all three groups and that fiber selection was random. There does seem to be fewer of the largest fibers ($> 10$ $\mu$m) in the homozygote than in the wild type, but this is most likely attributed to hypomyelination, because the original study found no evidence for any other axonal abnormalities (Henry et al., 1991). Thus, the decreased internodal distance observed in *clp* appears to result solely from the effects of the delayed myelination phenotype.

## DISCUSSION

Myelin marker staining of sciatic nerve cross-sections from heterozygous and homozygous mice gave the pattern one might expect for a recessive, delayed myelination mutant. The P14 heterozygote fiber staining showed a normal distribution of all three fiber markers studied. Using the P14 heterozygote as a basis for comparison, the P14 homozygote cross-sections had an abnormal appearance; both MAG and P0 immunoreactivities were decreased, whereas NCAM staining was increased. This observation suggests that most of the fibers in the P14 homozygote were stalled in an unmyelinated stage, with relatively few fibers going through the process of myelination. Once initiated, the myelination process itself appeared to be unaffected by the *clp* mutation, because all three fiber markers were in their proper location and sequence. Notably, MAG expression preceded P0 expression in *clp* myelination just as in wild type (Martini et al., 1988; Owens and Bunge, 1989).

Sodium channel and MAG staining in P14 sciatic nerve whole mounts corroborated the results from cross-sections. The P14 heterozygote had a mature staining pattern with MAG and sodium channel antibodies. The MAG staining pattern of the P14 homozygote showed that myelination was still in its early stages, with very few Schwann cells staining for MAG. Those Schwann cells that were MAG-positive were typically isolated and expressed MAG in a linear manner. When colabeled, the sodium channels were found in diffuse clusters at the ends of the MAG-positive Schwann cells and distributed throughout some of the

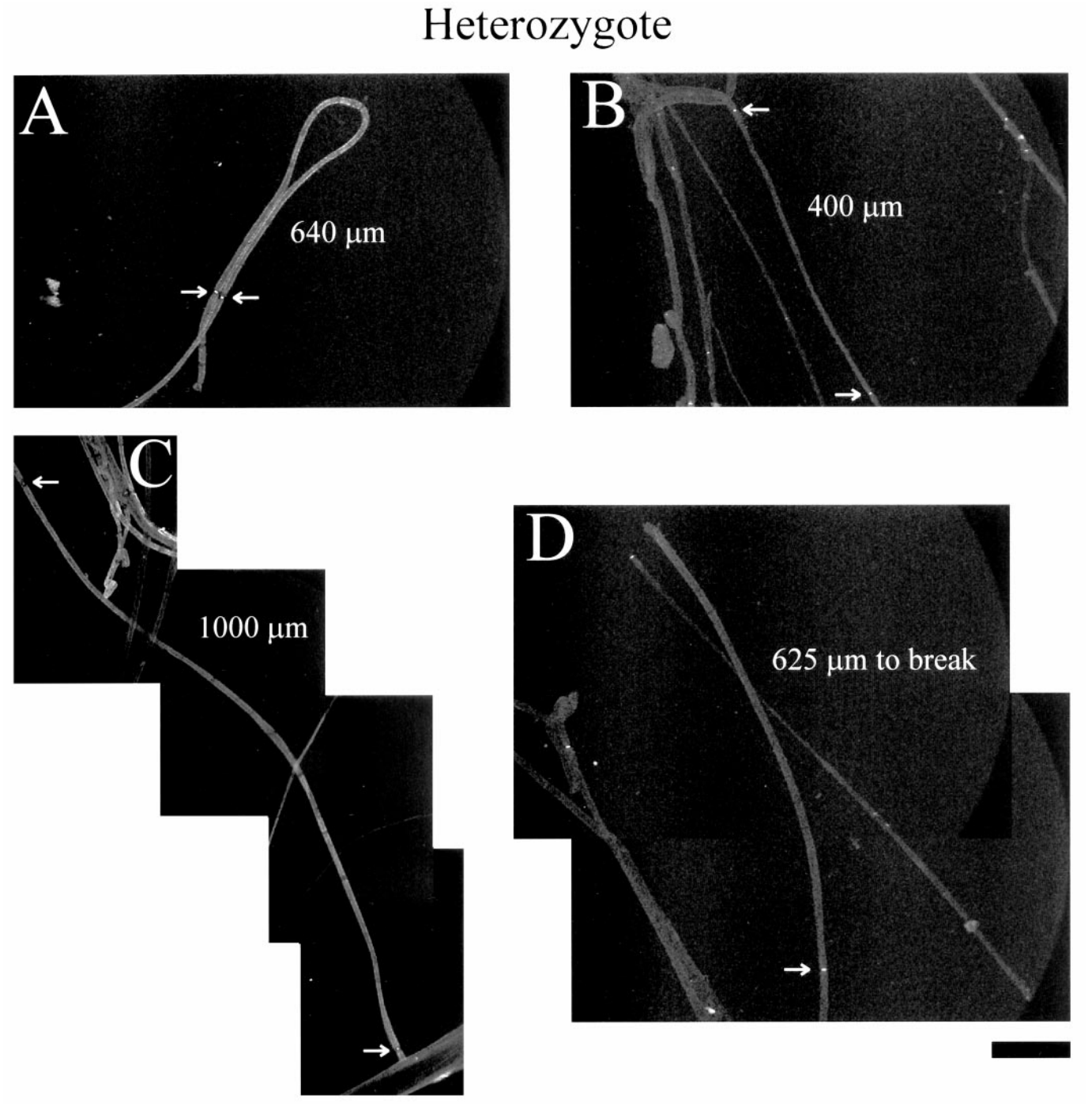


*Figure 4.* Adult heterozygote sciatic nerve whole mounts. Sodium channel immunoreactivity of whole-mount sciatic nerves from heterozygous adult mice is shown. *Arrows* point to nodes of Ranvier; internodal lengths measured between *arrows* in *A–C* are given. In *D*, the distance from the marked node to the break is given. Scale bar, 100 μm.

MAG-negative regions. All of the fiber-related sodium channel clusters found were in proximity to a MAG-positive Schwann cell.

These results are very similar to those reported in studies of sodium channel distribution in the developing and remyelinating rat sciatic nerve. Using lysolecithin-induced demyelination, it was found that sodium channel clusters appeared near the ends of adhering Schwann cells and were inferred to move with the Schwann cell during elongation until adjacent clusters fused into a mature node of Ranvier (Dugandzija-Novakovic et al., 1995; Novakovic et al., 1996). In developmental studies, sodium channel clusters were again found at the edges of Schwann cells determined to be in the early stages of myelination because of linear MAG staining (Vabnick et al., 1996). All axon-related sodium channel clusters were found in proximity to a MAG-positive Schwann cell. The striking similarity between these results and our studies of mouse *clp* sciatic nerves supports the hypothesis that myelinating Schwann cells determine the position of nodes of Ranvier.

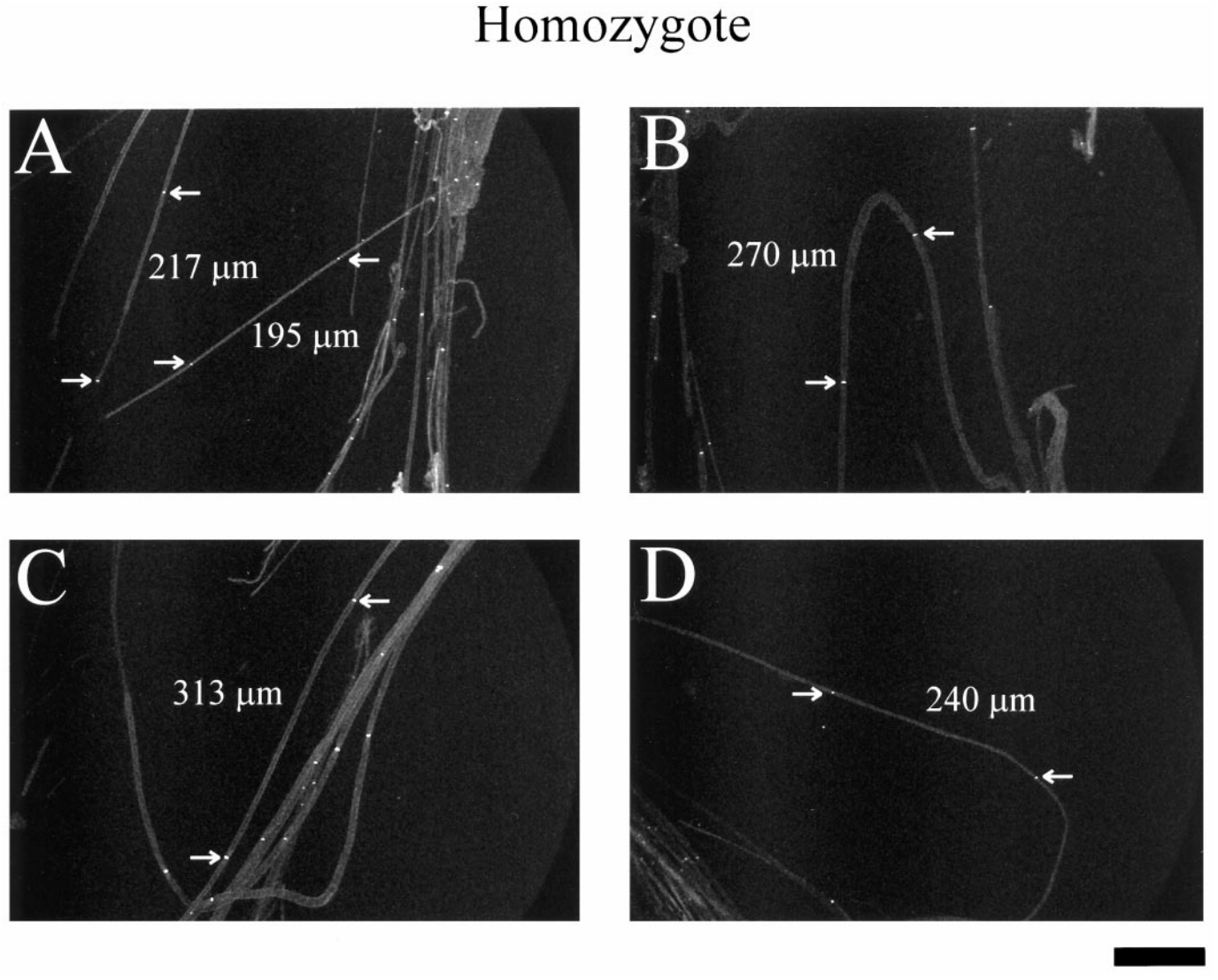


*Figure 5.* Adult homozygote sciatic nerve whole mounts. Sodium channel immunoreactivity of whole-mount sciatic nerves from homozygous adult mice is shown. *Arrows* point to nodes of Ranvier; internodal lengths measured between *arrows* in *A–D* are given. Scale bar, 100 μm.

**Table 1. Mean internodal lengths from node-to-node measurements of adult heterozygote and homozygote whole-mount sciatic nerves**

| Tissue | m.m.i.l. (μm)[a] | SD | No. of fibers |
|---|---|---|---|
| Heterozygote | 647 | 203 | 7 |
| Homozygote | 232 | 42 | 18 |

[a]m.m.i.l., Measured mean internodal length.

**Table 2. Mean internodal length calculations from nodal frequencies of adult heterozygote and homozygote whole-mount sciatic nerves**

| Tissue | Total fiber length (μm) | Total nodes | m.i.l. ± SD (μm)[a] |
|---|---|---|---|
| Heterozygote | 101,500 | 108 | 940 ± 90 |
| Homozygote | 69,378 | 236 | 296 ± 19 |

[a]m.i.l., Mean internodal length calculation from nodal frequency.

Further support for this hypothesis was found when we analyzed adult *clp* sciatic nerve internodal lengths. Homozygous mice had dramatically shortened internodal lengths. However, the magnitude of the difference between the heterozygote and homozygote depended on the data collection technique. Node-to-node measurement data yielded a shorter internodal length for the heterozygote; however, it agreed well with previous work. Friede and Beuche (1985) used a similar technique from the same region of mouse sciatic nerve and reported an average internodal length of 693 ± 124 μm, compared with our measurement of 647 ± 203 μm. By calculating mean internodal length from total fiber length and total number of nodes counted, broken fibers could be included in the data, yielding 940 ± 90 μm for the heterozygote.

There are several assumptions made when using this statistical technique. The first is that fiber breakage occurred in random locations. This assumption may not be entirely valid, because fibers may have a tendency to break at nodes of Ranvier because there is no myelin there (see Figs. 4*D*, 5*B*). However, this nonrandom breakage is not a problem as long as the likelihood of leaving the nodal axolemma itself on the slide to be counted is random. A second assumption made is that the fibers selected

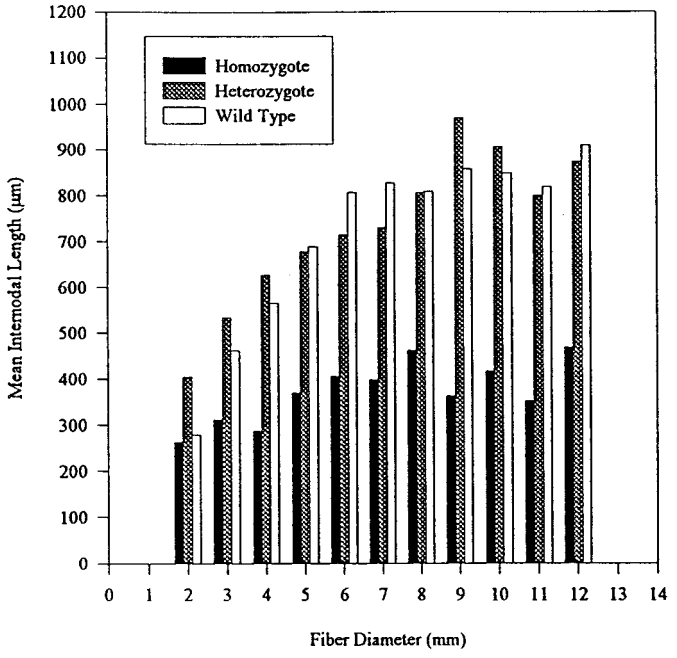


*Figure 6.* Histogram of fiber diameter versus internodal length for homozygote, heterozygote, and wild-type sciatic nerve whole mounts.

were a random sample of the population, especially in terms of fiber diameter. If larger-diameter fibers were more likely to separate as individual fibers or less likely to break, then this might bias the results. Thus, fiber diameters were measured along with total fiber length and number of nodes, showing that there was no significant bias and that a representative fiber population had been selected.

Regardless of the method used, we observed that *clp* mice had dramatically shorter internodal lengths than their heterozygote counterparts. What is the significance of altered internodal length to questions about nodal specification? Internodal length is the ratio of axon length to the number of myelinating Schwann cells. In development, the axon continues to extend after it becomes myelinated. It is thought that existing myelinating Schwann cells elongate with the growing axon; therefore, internodal distances increase until maturity (Schlaepfer and Myers, 1973; Friede et al., 1981). On the other hand, short internodal lengths occur in situations in which axon length is fixed, such as in the remyelination of a denuded adult axon. We suggest that shortened internodal lengths in *clp* peripheral nerves occurs as a result of the same process that causes shortened internodal lengths after demyelination: limited axonal growth after a delayed initiation of myelination. Overall, shortened internodes after remyelination and observations of sodium channel clustering at the edges of myelinating Schwann cells at all phases of elongation suggest that myelinating Schwann cells determine the location of new nodes of Ranvier.

A caveat when studying remyelination is that there is loss of the original nodes, which may reset or change the system in some way. Demyelination is known to upregulate sodium channel numbers, and it is possible that these new channels are localized differently than the original, developmental channels (England et al., 1991). However, *clp* appears to have the same net result of shortened internodes without having a demyelinating stimulus or loss of original nodes. If axons alone specified nodal location, then one would expect a normal internodal length for the original nodes. Thus, shortened internodes in *clp* also support the hypothesis that myelinating Schwann cells determine the sites of nodes of Ranvier because the *clp* internodal distance seems to be dependent on Schwann cell growth and independent of intrinsic axon-related factors such as fiber diameter or length.

In contrast, the alternate hypothesis of axonal predetermination of nodal sites seems to require less parsimonious explanations of the findings presented here. To maintain this as a viable hypothesis, one must account for how the *clp* mutation simultaneously affects the independent processes of nodal site specification and myelination as postulated by this paradigm. There are two possibilities by which this might occur. First, the *clp* defect might involve a single gene product that lies at or upstream of a branch point in a hypothetical cascade of molecular events that coordinately initiates myelination and nodal site formation. Alternatively, *clp* could involve two distinct but genetically linked defects that separately affect myelination and nodal site formation. Regardless of such considerations, it would seem that characterization of the molecular basis for the *clp* defect would yield important information about the early steps in PNS myelination and nodal formation.

**Table 3. Mean internodal length, number, and percentage of fibers studied for each fiber diameter in adult homozygote, heterozygote, and wild-type whole-mount sciatic nerves**

| Fiber diameter (μm) | Homozygote | | Heterozygote | | Wild-type | |
|---|---|---|---|---|---|---|
| | m.i.l. ± SD (μm)[a] | No. of fibers/ % of fibers | m.i.l. ± SD (μm) | No. of fibers/ % of fibers | m.i.l. ± SD (μm) | No. of fibers/ % of fibers |
| 2 | 263 ± 83 | 4/5 | 406 ± 122 | 5/3 | 280 ± 89 | 4/3 |
| 3 | 312 ± 62 | 10/12 | 534 ± 101 | 14/10 | 462 ± 92 | 14/9 |
| 4 | 287 ± 41 | 15/18 | 628 ± 134 | 14/10 | 566 ± 103 | 18/12 |
| 5 | 369 ± 64 | 12/15 | 679 ± 110 | 28/19 | 689 ± 124 | 21/13 |
| 6 | 406 ± 71 | 15/18 | 716 ± 125 | 22/15 | 808 ± 158 | 17/11 |
| 7 | 397 ± 75 | 10/12 | 731 ± 177 | 13/9 | 829 ± 201 | 13/8 |
| 8 | 462 ± 109 | 6/7 | 808 ± 196 | 14/10 | 810 ± 169 | 15/10 |
| 9 | 362 ± 93 | 6/7 | 971 ± 217 | 21/14 | 859 ± 183 | 13/8 |
| 10 | 416 ± 147 | 3/4 | 907 ± 273 | 10/6 | 850 ± 125 | 26/16 |
| 11 | 350 ± 157 | 1/1 | 800 ± 302 | 5/3 | 819 ± 175 | 12/7 |
| 12 | 467 ± 270 | 1/1 | 875 ± 619 | 2/1 | 910 ± 407 | 4/3 |

[a]m.i.l., Mean internodal length calculation from nodal frequency.

There are cases in the PNS in which sodium channel clusters are found in the absence of Schwann cells. In all of these cases there is a state of chronic demyelination. Sodium channels in chronic demyelination appear to redistribute differently than in acute demyelination (England et al., 1996). These chronically demyelinated fibers may be able to make use of axonally specified ankyrin-binding proteins (Lambert et al., 1997) to form node-like structures. Myelinating Schwann cells, however, appear to have the ability to reorganize these binding protein clusters along with ankyrin and sodium channels—just the properties that cells would need to specify nodes of Ranvier.

Some questions that remain unanswered about this study revolve around the nature of the *clp* defect. The defect appears to involve the early interaction of Schwann cells and axons, so likely candidate proteins would be adhesion molecules such as MAG, NCAM, and L1. The MAG gene is located near the *clp* mutation on chromosome 7 (Barton et al., 1987; Henry et al., 1991); however, the correct positional and sequential expression of MAG suggests that the primary defect in *clp* is not in the coding region of the MAG gene itself. This hypothesis has been confirmed in a breeding experiment in which a MAG knock-out mouse was crossed with a *clp* homozygote mouse. If the *clp* mutation was not allelic to the MAG locus, then normal progeny would be expected because of complementation. All of the progeny from this cross had normal forelimb posture and normal MAG expression (G. C. Owens, C. Li, and J. R. Roder, unpublished observations). The NCAM gene maps to chromosome 9, and its expression pattern looks appropriate (D'Eustachio et al., 1985). L1 is X-linked, and its expression pattern was not studied (Djabali et al., 1990). The key to understanding the *clp* defect will be finding the mutated gene and determining its function. If this can be done, then our findings suggest that further insight may be forthcoming into the nature of axon–Schwann cell communication and its role in nodal development.

## REFERENCES


Barton DE, Arquint M, Roder J, Dunn R, Francke U (1987) The myelin-associated glycoprotein gene: mapping to human chromosome 19 and mouse chromosome 7 and expression in quivering mice. Genomics 1:107–112.

D'Eustachio P, Owens GC, Edelman GM, Cunningham BA (1985) Chromosomal location of the gene encoding the neural cell adhesion molecule (N-CAM) in the mouse. Proc Natl Acad Sci USA 82:7631–7635.

Deerinck TJ, Levinson SR, Bennett GV, Ellisman MH (1997) Clustering of voltage-sensitive sodium channels on axons is independent of direct Schwann cell contact in the dystrophic mouse. J Neurosci 17:5080–5088.

Djabali M, Mattei MG, Nguyen C, Roux D, Demengeot J, Denizot F, Moos M, Schachner M, Goridis C, Jordan BR (1990) The gene encoding L1, a neural adhesion molecule of the immunoglobulin family, is located on the X chromosome in mouse and man. Genomics 7:587–593.

Dugandzija-Novakovic S, Koszowski AG, Levinson SR, Shrager P (1995) Clustering of $Na^+$ channels and node of Ranvier formation in remyelinating axons. J Neurosci 15:492–503.

England JD, Gamboni F, Levinson SR (1991) Increased numbers of sodium channels form along demyelinated axons. Brain Res 548:334–337.

England JD, Levinson SR, Shrager P (1996) Immunocytochemical investigations of sodium channels along nodal and internodal portions of demyelinated axons. Microsc Res Tech 34:445–451.

Friede RL, Beuche W (1985) A new approach toward analyzing peripheral nerve fiber populations. I. Variance in sheath thickness corresponds to different geometric proportions of the internodes. J Neuropathol Exp Neurol 44:60–72.

Friede RL, Meier T, Diem M (1981) How is the exact length of an internode determined? J Neurol Sci 50:217–228.

Henry EW, Eicher EM, Sidman RL (1991) The mouse mutation *claw paw*: forelimb deformity and delayed myelination throughout the peripheral nervous system. J Hered 82:287–294.

Kaplan MR, Meyer-Franke A, Lambert S, Bennett V, Duncan ID, Levinson SR, Barres BA (1997) Induction of sodium channel clustering by oligodendrocytes. Nature 386:724–728.

Lambert S, Davis JQ, Bennett V (1997) Morphogenesis of the node of Ranvier: coclusters of ankyrin and ankyrin-binding integral proteins define early developmental intermediates. J Neurosci 17:7025–7036.

Martini R, Schachner M (1986) Immunoelectron microscopic localization of neural cell adhesion molecules (L1, N-CAM, and MAG) and their shared carbohydrate epitope and myelin basic protein in developing sciatic nerve. J Cell Biol 103:2439–2448.

Martini R, Bollensen E, Schachner M (1988) Immunocytological localization of the major peripheral nervous system glycoprotein P0 and the L2/HNK-1 and L3 carbohydrate structures in developing and adult mouse sciatic nerve. Dev Biol 129:330–338.

Novakovic SD, Deerinck TJ, Levinson SR, Shrager P, Ellisman MH (1996) Clusters of axonal $Na^+$ channels adjacent to remyelinating Schwann cells. J Neurocytol 25:403–412.

Owens GC, Bunge RP (1989) Evidence for an early role for myelin-associated glycoprotein in the process of myelination. Glia 2:119–128.

Salzer JL (1997) Clustering sodium channels at the node of Ranvier: close encounters of the axon-glia kind. Neuron 18:843–846.

Schlaepfer WW, Myers FK (1973) Relationship of myelin internode elongation and growth in the rat sural nerve. J Comp Neurol 147:255–266.

Sternberger NH, Quarles RH, Itoyama Y, Webster HD (1979) Myelin-associated glycoprotein demonstrated immunocytochemically in myelin and myelin-forming cells of developing rat. Proc Natl Acad Sci USA 76:1510–1514.

Vabnick I, Novakovic SD, Levinson SR, Schachner M, Shrager P (1996) The clustering of axonal sodium channels during development of the peripheral nervous system. J Neurosci 16:4914–4922.

Waxman SG (1978) Variations in axonal morphology and their functional significance. In: Physiology and pathobiology of axons (Waxman SG, ed), pp 169–190. New York: Raven.